Journal of Molecular Graphics and Modelling 44 (2013) 9–16

Contents lists available at SciVerse ScienceDirect

Journal of Molecular Graphics and Modelling

journal homepage: www.elsevier.com/locate/JMGM

MD and QM/MM study on catalytic mechanism of a FAD-dependent enzyme ORF36: For nitro sugar biosynthesis

Yanwei Li, Lei Ding, Qingzhu Zhang*, Wenxing Wang

Environment Research Institute, Shandong University, Jinan 250100, PR China

ARTICLE INFO

Article history:
Accepted 24 April 2013
Available online 14 May 2013

Keywords:
Everninomicin
Molecular dynamics
Mechanical/molecular mechanical method
Hydroxylation
Electrostatic influence

ABSTRACT

The catalytic mechanism of a FAD-dependent nitrososynthase (ORF36) was studied with molecular dynamics (MD) and quantum mechanical/molecular mechanical (QM/MM) methods. Residues Leu160 and Phe374 play an important role during the FAD binding with ORF36. Similar phenylalanine/leucine pair was found in the other two enzymes of this family. For the second oxidation step of ORF36 toward thymidine diphosphate-L-*epi*-vancosamine, three elementary catalytic steps were found: a hydroxylation step, a hydrogen back-transfer step and a hydroxyl group elimination step. The hydroxylation step is found to be the rate-determining step with an energy barrier of 26.3 kcal/mol under the B3LYP/cc-pVTZ//CHARMM22 level. Two possible pathways for the second oxidation step are carefully investigated. Our simulations indicate that an oxygen atom from the coenzyme FADHOOH is inserted into the product. In addition, the electrostatic influence of 17 individual residues and five neighboring water molecules on the rate-determining step was estimated. The results indicate that groups Gly132/Ala133/Leu134, Met375/Gln376 and a water fence play a key role in facilitating the rate-determining step. On the other hand, residues Leu160, Val161 and Ser162 are found to be critical to suppress the rate-determining step. Our results lead to further understanding of the detailed catalytic pathways for nitro sugar biosynthesis.

1. Introduction

Everninomicin is a broad-spectrum efficacy antibiotic against multidrug resistant enterococci and *Staphylococcus aureus* [1,2]. It has also been considered as one of the new therapeutic medical candidates for treating Legionnaires' disease [3]. Due to the decreased reproductive performance observed in pregnant female rats [4], it is terminated in phase three clinical trials. As limited antibiotics share the similar efficacy with everninomicin [5], exploring its analogs.for clinical use becomes important. The nitro sugar moiety of everninomicin is believed to be crucial for its extraordinary antibiotic characteristic [6]. As a result, it is critical to understand the biosynthesis progress of nitro sugar moiety [7,8].

Enzyme ORF36 which belongs to the class D flavoprotein monooxygenase is involved in the biosynthesis process of nitro sugar moiety. It shows great potential in the application of pharmaceutical, finechemical and food industries [9,10]. ORF36 (firstly crystallized in 2010) is observed to catalyze the two-step oxidation of thymidine diphosphate (TDP)-L-*epi*-vancosamine, an analog of TDP-L-evernitrosamine or TDP-L-evernitrose (precursors of everninomicin) [11]. The relative structures and their relations are provided in Scheme 1. The ^{18}O incorporation studies have been performed to learn its catalytic mechanism [11]. The studies revealed that the molecular oxygen rather than oxygen from water was incorporated into the substrate. However, there are still several unsolved important questions: Does the ^{18}O in the product come from the first oxidation step or from the second oxidation step? What is the detailed mechanism of the second oxidation step? Are there more than one elementary reaction in the second oxidation step, and which one is rate-determining? How do the neighboring residues influence the oxidation reaction? Can there be any mutations to increase the efficiency of ORF36? All these questions cannot be easily answered in the experiment.

Quantum mechanical/molecular mechanical (QM/MM), a newly developed method for biological systems, has received widespread acceptance [12]. There are several successful QM/MM studies on *p*-hydroxybenzonate hydroxylase (a kind of flavoprotein monooxygenase) [13–15]. Thus, it is reasonable and accurate enough to investigate the catalytic mechanism of enzyme ORF36 by using QM/MM method. No similar theoretical studies on the catalytic mechanism of ORF36 or its highly identical enzymes have been performed. Hence, QM/MM simulations performed in this article will supplement the experimental results and provide a theoretical base for the further study of nitro sugar biosynthesis.

* Corresponding author. Tel.: +86 0531 88369787; fax: +86 531 8836 1990.
E-mail address: zqz@sdu.edu.cn (Q. Zhang).

1093-3263/$ – see front matter © 2013 Elsevier Inc. All rights reserved.
http://dx.doi.org/10.1016/j.jmgm.2013.04.008

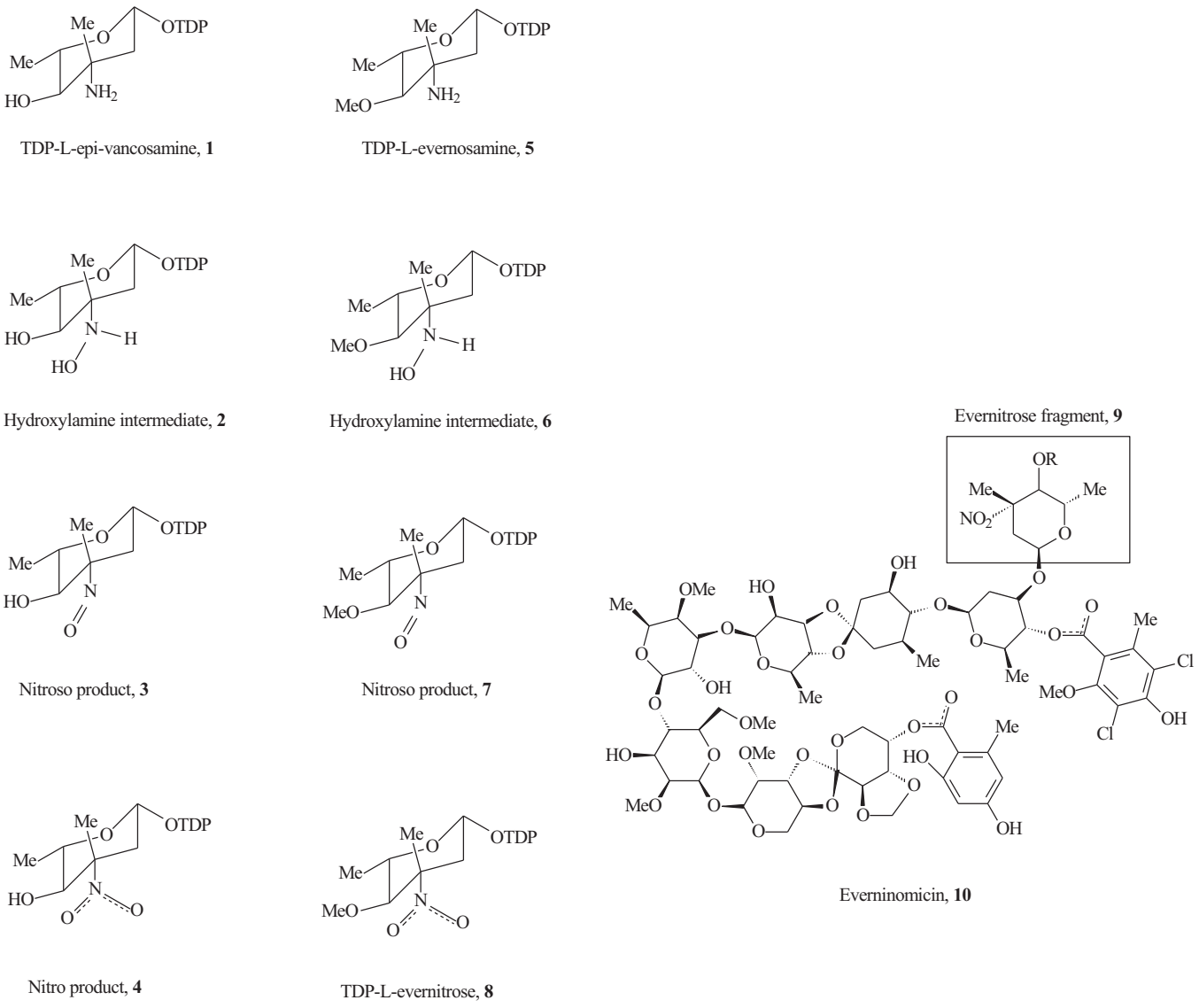

Scheme 1. Structures and relations of TDP-L-evernitrosamine and its analogs.

2. Computational methods

2.1. Initial models

The initial models of ORF36 (model M-A), KijD3 (model M-B) and isobutyryl-CoA dehydrogenase (IBD, model M-C) were constructed on the basis of the X-ray crystal structures obtained from Protein Data Bank (PDB ID: 3MXL, 3M9V and 1RX0) [11,16,17]. Due to the high identical conformations and orientations of FAD in different crystal structures (Fig. S1), we can speculate that the conformation and orientation of FAD in enzyme ORF36 will be the same. Thus, the structure of FAD in PDB ID 2JIF was extracted for docking to ORF36 because of its highest protein identity compared with ORF36. FAD and TDP were docked to ORF36 (model M-D) by using the receptor-ligand interactions module (CDOCKER) in program Accelrys Discovery Studio 2.1 (Accelrys Software Inc.). The obtained results are in agreement with the previously reported binding mode [11]. Ser162 and His92 are conformed to form a hydrogen bond with FAD and the substrate. The protonation state of the active site residues in each model was manually checked by using VMD [18] program. The missing hydrogen atoms in the X-ray structure were added through the HBUILD facility in the CHARMM package (version c33b1) [19–21].

2.2. Classic molecular dynamics simulations

CHARMM22 force field [22] was used during MD simulations. Taking model M-A as an example, the ORF36 and all the crystal water molecules were kept unchanged when being merged in a cubic box with 27,000 TIP3P water molecules [23]. The water molecules overlapping within 2.5 Å of ORF36 were deleted. The whole system was neutralized with seven sodium ions and minimized for 10,000 steps with no constrains. Then the cubic box was modified to a sphere with the diameter 90 Å. After that, the system was heated from absolute zero to 298.15 K in 50 ps (1 fs/step) and equilibrated thermally for 500 ps (1 fs/step) to reach the equilibration state. The Stochastic Boundary molecular dynamics method (SBMD) has been used to mimic the aqueous environment during the 10 ns simulation [24]. Partitions of the system are labeled as follows: within 34 Å of the sphere is defined as reaction zone, within 34–43 Å of the sphere is defined as buffer zone, the rest of the system atoms are defined as reservoir. The reservoir zone is not included in the dynamics simulations, however, a deformable potential was imposed at the edge of the sphere to mimic the effect of the water solvent. Since the reservoir can guarantee the constant system volume, the approach of the canonical ensemble (NVT, 298.15 K) was achieved. The leap-frog algorithm and Langevin

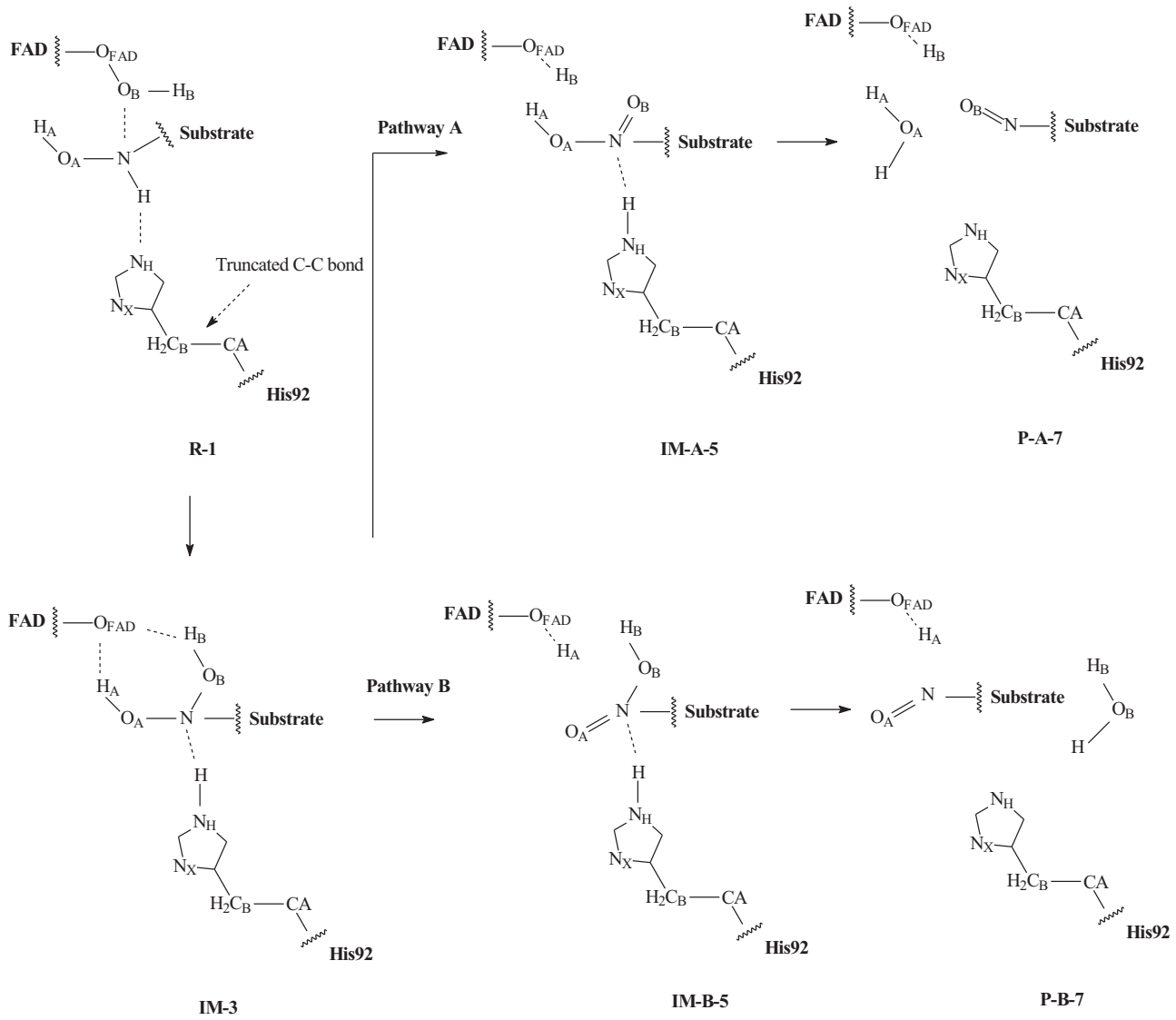

Scheme 2. Catalytic reaction scheme of ORF36, atoms mentioned in the text are labeled.

temperature coupling method implemented in CHARMM were applied during the simulation. Same strategy was adopted for model M-B and M-C. The temperature and total energy variations of these three models are shown in Figs. S2–7. The average temperature of these models (M-A to M-D) are 297.61 K, 297.56 K, 297.67 K, and 297.52 K, respectively. They are close to the thermostat temperature 298.15 K (within 0.7 K). For model M-D, FAD and TDP were constrained using "CONStraint HARMonic FORCE" command in CHARMM scripts during the 2 ns MD simulation. This makes the atoms of FAD or TDP move to some extent. This method is useful in keeping their overall structures. According to the temperature and total energy variations (Figs. S8 and S9) and the structure differences between the average structure and the last structure (Fig. S10), the whole system has reached the stable state after 2 ns simulation.

2.3. QM/MM setup

The second oxidation step of ORF36 was investigated with QM/MM method. The calculations were performed by using ChemShell [25] platform. It can perfectly integrate programs Turbomole [26] and DL-POLY [27]. Together with charge shift model [28], an electronic embedding [29] where MM charges polarize the QM region were used for QM/MM calculation. The QM-region was treated by DFT with B3LYP functional [30,31], while the CHARMM22 force field [32] was used for the MM-region. The geometry optimizations were optimized under B3LYP/6-31G(d)//CHARMM22 level with hybrid delocalized internal coordinates (HDLC) [33] optimizer. In these calculations, 1506 SCF-basis functions were included. A large basis set cc-pVTZ was used for single point energy calculations. The potential energy surfaces (PES) were scanned to determine the exact transition state. Key bond distances between the reacting atoms were fixed in each step (point) of the scans. The structure of the highest energy point along the PES was extracted and further optimized to ensure its transition state characteristic. Transition state searches were done with the microiterative TS optimizer which combines partitioned rational function optimizer (P-RFO) algorithm [34] and the low-memory Broyden–Fletcher–Goldfarb–Shanno (L-BFGS) algorithm [35]. Both of the algorithms are implemented in the HDLC optimizer of ChemShell. By using the method which has been successfully applied in a former study [36], the system is split into a reaction core containing very few atoms and the environment to accelerate TS searches with less computing cost. Fifteen core atoms were defined as core atoms in this study (Fig. S11). It is worth mentioning that all the movable atoms (QM and MM) were considered in

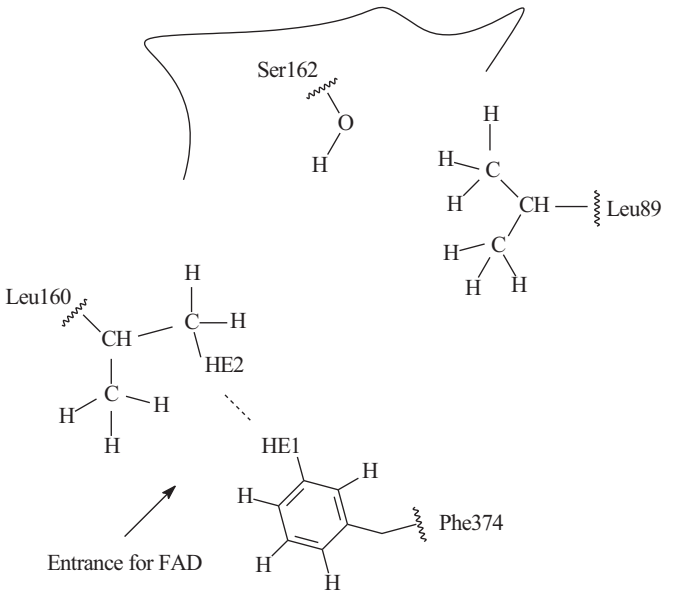

Scheme 3. Crucial residues and the binding entrance of ORF36 for FAD.

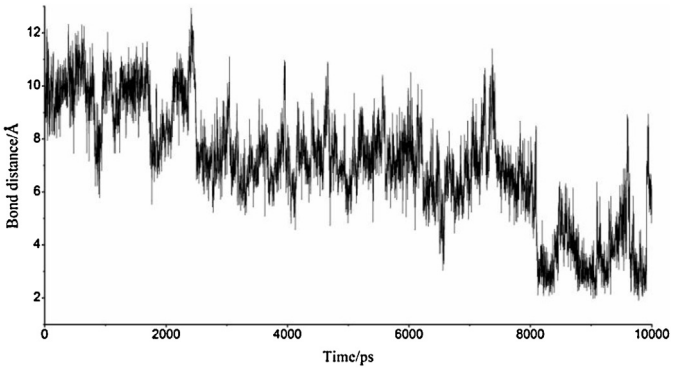

Fig. 1. Bond distance variation (HE1—HE2) along the 10 ns simulations of model M-A. The labels of HE1 and HE2 are provided in Scheme 3.

locating the final TS structure. Harmonic vibrational frequency calculations were also performed for all the QM atoms by using the force module to validate the one imaginary frequency and a suitable transition vector. Vibrational frequency calculations on reactants and products were also performed to determine the zero-point energy (ZPE).

The QM-region contains coenzyme FAD, substrate TDP and the functional group of His92. His92 was truncated by cutting the C—C bond (shown in Scheme 2) and was then complemented by a hydrogen link atom. This resulted in 162 QM atoms and one hydrogen link atom. Why such a big QM-region was selected is based on two reasons: to accurately evaluate the geometries of FAD and TDP during the catalytic reaction; to obtain the detailed information of the reaction mechanism. Atoms within 20 Å of atom N (shown in Scheme 2) were allowed to adjust their positions, resulting in 3617 movable atoms. Other atoms in the system were fixed during the QM/MM calculation.

2.4. Electrostatic influence of a single amino acid

The activation energy difference caused by amino acid *i* can be described as:

$$\Delta E^{0-i} = \Delta E^{i} - \Delta E^{0} \quad (1)$$

Where ΔE^{0-i} is the energy changes of the barrier, ΔE^{i} is the energy barrier with charges on residue *i* set to 0, and ΔE^{0} is the original values of the energy barrier. During all these energy calculations, the geometry structures of the stationary points were kept unchanged. A positive ΔE^{0-i} value means the *i*th residue stabilizes the transition state more than reactant.

3. Results and discussion

3.1. Influence of key residues on FAD docking process

Although the electron density map of FAD and the substrate could not be identified [11,16], crystal structures of ORF36 (PDB ID: 3MXL) and KijD3 (PDB ID: 3M9V) were in the "Enzyme-FAD-substrate" binding state. In general, there are mainly two pockets in these FAD-dependent enzymes: one is for FAD binding and the other is for substrate binding. According to our calculation, Ser162 binds with the isoalloxazine ring of FAD through a hydrogen bond. This is in agreement with the former study [11]. By carefully investigating the environment residues for FAD binding from the 10 ns MD trajectory, the importance of residues Ser162, Leu89, Leu160, and Phe374 were found. Their relative positions were provided in Scheme 3. As indicated in Scheme 3, FAD should firstly go through the channel (buildup by residues Leu89, Leu160, and Phe374) to finally binds with Ser162. Snapshots were extracted every 0.5 ns from the 10 ns MD trajectory to roughly represent the movements of these residues. (Fig. S12). The detailed distance (HE1–HE2) variation between residue Leu160 and Phe374 was shown in Fig. 1. The distance decreases in 2–3 ns (from about 10.0 Å to 7.0 Å) and 7–8 ns (from about 7.0 Å to 3.0 Å), and it stays relatively stable in 8–10 ns. This indicates a process that residues Leu160 and Phe374 gradually approach each other during the 10 ns simulations. B-factor of the residues of ORF36 was also provided (Fig. S13).

KijD3 is an enzyme with the highest identity (64%) with ORF36 among all the crystallized FAD-dependent monooxygenases [11]. Residue Ser171 is found to bind with FAD through a hydrogen bond [16]. By carefully studying the binding pocket for FAD, residues of Leu98, Leu169, and Phe383 were highlighted and their relative positions were provided in Fig. S14. The 20 extracted snapshots from the 10 ns simulation were depicted in Fig. S15. The detailed distance variation (HE2–OE) between residue Leu169 and Phe383 was shown in Fig. S16. The distance decreases in 1–2 ns (from about 7.5 Å to 5.5 Å), 3–4 ns (from about 6.0 Å to 4.0 Å) and 8–9 ns (from about 5.5 Å to 4.0 Å). This indicates that residues Leu169 and Phe383 gradually approach each other during the 10 ns simulations. B-factor of all the residues of KijD3 was provided in Fig. S17.

Like enzymes ORF36 and KijD3, Ser171 binds with FAD of enzyme IBD through a hydrogen bond [17]. As indicated in Figs. S18 and S19, FAD should firstly go through the channel (buildup by residues Thr139, Phe169, Trp216 and Leu375) to finally binds with Ser171. By investigating the different distance variations (HB1–HD2, HE3–HD3, HE2–HD1 and HE1–HD1), the results show that distance HE3–HD3 is the shortest (about 3 Å, Fig. S20). Thus, residues Phe169 and Leu375 are more important than residues Thr139 and Trp216. In the last 1 ns trajectories, the OH group of Ser171 turns to the inner side of IBD to avoid being bounded by other homologues of FAD. This also indicates that once FAD binds with IBD, it may also induce the turning of the OH group from the inner side to the outer side. Flexibility (indicated by B-factors) of IBD in water was provided in Fig. S21.

Two crucial residues in ORF36 (Leu160 and Phe374), KijD3 (Leu169 and Phe383) and IBD (Phe169 and Leu375) were found in the three studied enzymes. The results indicate that a phenylalanine/leucine pair or similar residue pairs might be important for FAD binding. Of course, huge amount of studies should be

Table 1
Key bond distances in Å during the catalytic reaction.

		O_{FAD}—O_B	O_B—N	N—H	H—N_H	O_{FAD}—H_B	O_B—H_B	O_A—H	O_A—N	O_A—H_A	O_{FAD}—H_A	O_B—H
	R-1	1.50	3.08	1.03	2.06							
	TS-2	1.98	1.85	1.05	1.77							
	IM-3	2.59	1.47	1.73	1.06							
Path A	IM-3		1.47	1.73	1.06	1.57	1.04	2.66	1.50			
	TS-A-4		1.54	1.54	1.12	1.04	1.52	2.48	1.60			
	IM-A-5		1.37	1.49	1.13	1.03	1.58	2.38	1.61			
	TS-A-6		1.36	1.54	1.11		1.56	2.31	1.65			
	P-A-7		1.25	2.47	2.07		2.11	2.07	2.66			
Path B	IM-3		1.47	1.73	1.06				1.50	1.03	1.66	2.69
	TS-B-4		1.48	1.74	1.06				1.50	1.12	1.38	2.69
	IM-B-5		1.50	1.57	1.10				1.43	1.60	1.04	2.53
	TS-B-6		1.99	2.98	1.05				1.30	1.88		1.60
	P-B-7		2.72	2.87	4.41				1.25	2.15		0.99

performed to verify whether this kind of residue pair exists in other enzymes of this family.

3.2. Catalytic mechanism and energy profile

The catalytic mechanism of the second oxidation step of ORF36 consists of three elementary steps: (1) the hydroxyl transfer from coenzyme FADHOOH to the substrate, known as hydroxylation step; (2) a hydrogen back-transfer from the substrate to $FADHO^-$ and (3) elimination of hydroxyl group from the substrate to form the final product. Key bond distance variations during the reaction path are given in Table 1. Energy profile along the catalytic reaction is calculated under level B3LYP/cc-pVTZ//CHARMM22 plus ZPE correction (Fig. 1).

The hydroxylation step is accomplished through heterolytic cleavage of O_{FAD}—O_B bond, cleavage of N—H bond and formation of bonds O_B—N and H—N_H. Atom labels used in the following paragraphs are described in Scheme 2. The hydroxylation step can be described as follows: firstly, polarization of N—H bond by His92 makes N atom more nucleophilic; secondly, the nucleophilic N atom directly influences the electron distribution of O_{FAD}—O_B bond and finally causes its heterolytic cleavage. The energy barrier of the hydroxylation step is the highest along the reaction pathway (~26.3 kcal/mol, ZPE correction considered) which shows the rate-determining characteristic of the hydroxylation step. Although most of the enzymatic energy barriers are lower than 25 kcal/mol, there are still some studied barriers higher than this value. Some are even greater than 30 kcal/mol (32 kcal/mol, [37]) (36 kcal/mol, [38]). It is likely that energy barrier varies greatly among different enzyme species. Thus, the energy barrier (26.3 kcal/mol) in our study is acceptable for a enzymatic reaction. Additionally, the free energy of the reaction was not considered, which requires very time-consuming QM/MM molecular dynamic simulations to sample phase space. And this usually lower the reaction barrier by a few kcal/mol. The structure feature of TS-2 is shown in Fig. 2.

The structure of hydrogen back-transfer step (IM-3) is shown in Fig. 2. In IM3, there are two hydrogen bonds between substrate TDP and coenzyme FAD (H_A—O_{FAD}, 1.66 Å; H_B—O_{FAD}, 1.57 Å). This indicates that both H_A and H_B are likely to be transferred to O_{FAD}. As a result, there are two possible pathways of hydrogen back-transfer process. A pathway with O_{FAD}—H_B bond formation and O_B—H_B bond cleavage in defined as pathway A. On the other hand, O_{FAD}—H_A bond forms and O_A—H_A bond breaks in pathway B. The relatively low energy barriers in pathway A and pathway B (0.1 kcal/mol and 0.6 kcal/mol) show that the reaction happens easily. The exothermic characteristic in pathway A ($\Delta H_A = -3.0$ kcal/mol) and pathway B ($\Delta H_B = -14.3$ kcal/mol) indicate IM-3 is unstable

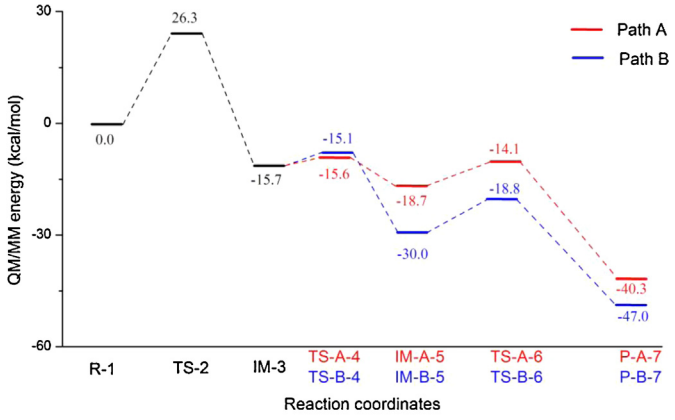

Fig. 2. Energy profile along the catalytic reaction of ORF36 under level B3LYP/cc-pVTZ//CHARMM22 plus ZPE correction.

compared with IM-A-5 and IM-B-5 and can be hardly detected in the experiment. The structure features of TS-A-4, TS-B-4, IM-A-5, and IM-B-5 were provided in Figs. S22 and S23.

The elimination step is the key step to determine the favored pathway. His92 gradually moves toward group O_A—H_A in pathway A, making N—O_A bonds more breakable. This movement finally leads to the formation of a water molecule (H_2O, H_A—O_A—H). While in pathway B, His92 influences the electron distribution of bond N—O_B, making H atom of His92 approaches group O_B—H_B. This finally leads to the N—O_B bond cleavage and formation of a water molecule (H_2O, H_B—O_B—H_B). Considering ZPE correction, the energy barriers of pathway A and pathway B are 4.6 kcal/mol and 11.2 kcal/mol. Lower energy barrier of pathway A guarantees that it is more feasible. This means O_B atom, which comes from the coenzyme FADHOOH, is inserted into the product. The energy differences between R-1/P-A-7 and R-1/P-B-7 indicate that both reaction paths are exothermic ($\Delta H_A = -40.3$ kcal/mol, $\Delta H_B = -47.0$ kcal/mol). This guarantees that the catalytic reaction is irreversible. The structure features of TS-A-6, TS-B-6 are shown in Fig. 3. The structures of P-A-7 and P-B-7 were provided in Fig. S24.

3.3. Influence of individual residues on the rate-determining step

The electrostatic influence of His92 is not studied because it is included in QM region. The electrostatic influence of many other key individual residues on the rate-determining step was estimated. During the electrostatic influence study, the optimized

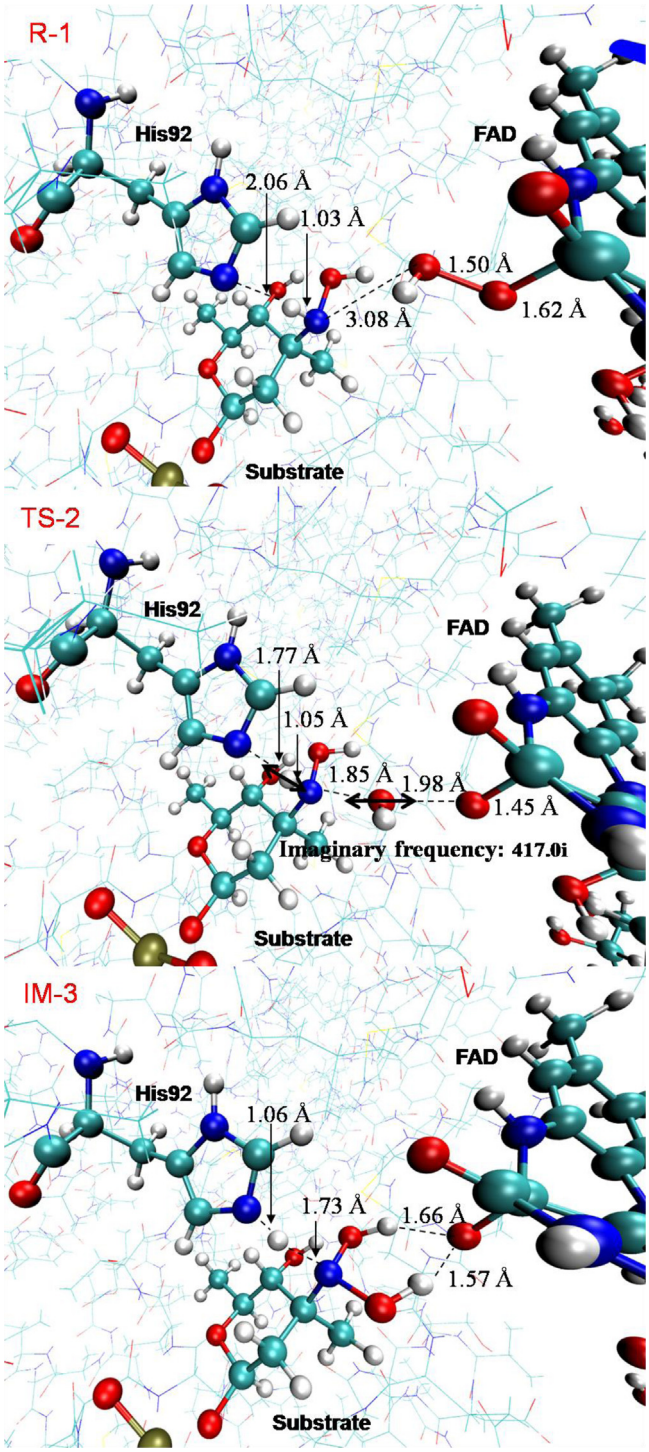

Fig. 3. Optimized structures of R-1, TS-2 and IM-3 at the B3LYP/6-31G(d)//CHARMM22 QM/MM level. The vibrational mode of the imaginary frequency of TS-2 is indicated by double sided black arrows.

reactant and transition state structures were kept unchanged. The stabilizing factor (positive ΔE^{0-i} value means the ith residue stabilizes the transition state more than reactant) of seventeen key residues and five water molecules were provided in Fig. 4. For all the individual residues investigated, Ser162 suppresses the hydroxylation reaction most, while Leu134 and Gln376 contribute equally in facilitating it. Groups Gly132/Ala133/Leu134 and Met375/Gln376 slightly facilitate the hydroxylation reaction, while group Leu160/Val161/Ser162 hampers it (Table 2). A water fence

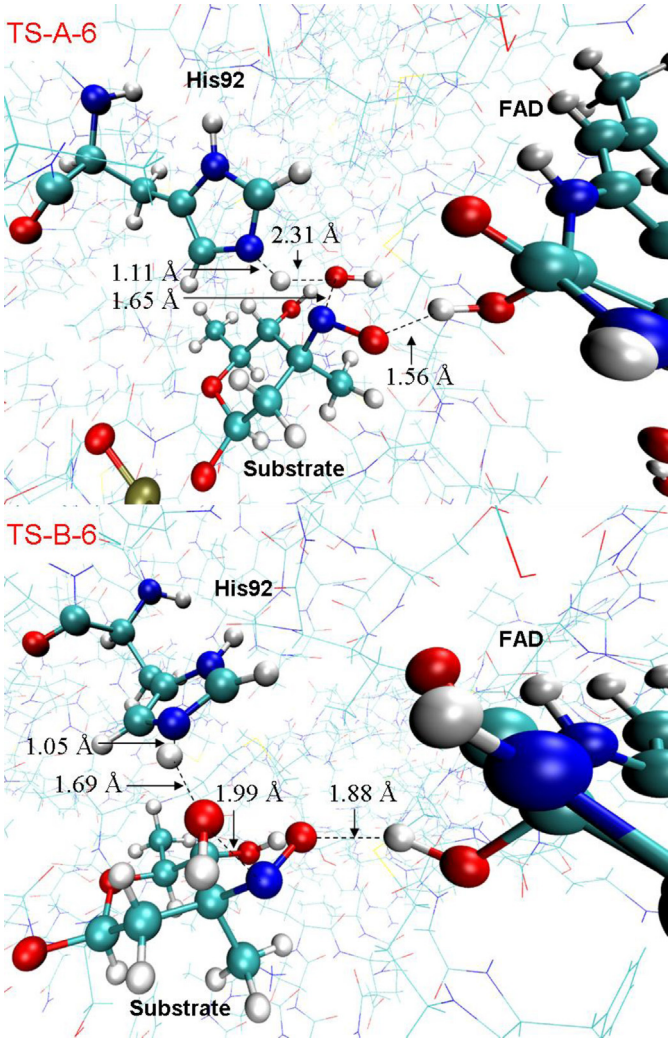

Fig. 4. Optimized structure of TS-A-6 and TS-B-6 at the B3LYP/6-31G(d)//CHARMM22 QM/MM level.

Table 2
Electrostatic influence of a single residue on activation barrier of TS-2.

Residue *i*	Charge	ΔE^{0-i} (kcal/mol) R-1 to TS-2
LEU89	0	0.9
VAL93	0	0.2
SER96	0	0.1
ARG97	+1	1.0
GLY132	0	−0.7
ALA133	0	1.3
LEU134	0	1.7
LEU160	0	−2.3
VAL161	0	−0.2
SER162	0	−3.1
GLN245	0	0.2
SER248	0	0
SER249	0	−0.4
THR251	0	0.9
MET252	0	−0.3
MET375	0	1.3
GLN376	0	1.7
PRO377	0	−0.5
WAT2925	0	7.8
WAT3702	0	−4.9
WAT3713	0	4
WAT4460	0	−5.9
WAT4465	0	2.1

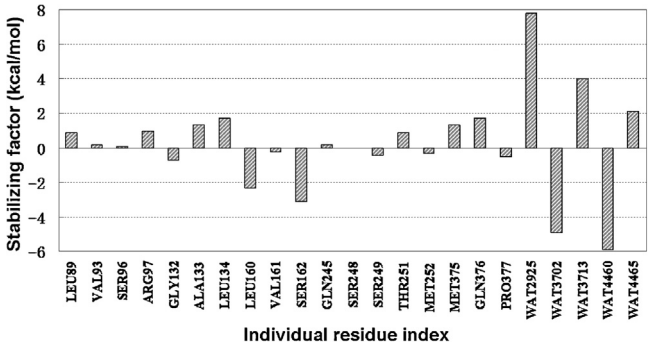

Fig. 5. Influence of individual residues on the rate-determining step.

consists of five water molecules slightly facilitates hydroxylation reaction. We hope this electrostatic influence study to be helpful for the experimental mutation studies (Fig. 5).

4. Conclusions

The catalytic mechanism of ORF36 was studied by using MD and QM/MM approaches. Key residues that influence the FAD binding to ORF36 were investigated by using MD method. Similar residues and their functions were also found in FAD-dependent enzymes KijD3 and IBD. A phenylalanine/leucine pair was found to be crucial in suppressing the FAD binding in the three studied enzymes. According to our QM/MM results, several conclusions can be drawn from this study: (1) The second oxidation step of ORF36 consists of three elementary steps: hydroxylation step, hydrogen back-transfer step, and hydroxyl group elimination step. (2) The hydroxylation step was found to be the rate-determining step. (3) O_B atom which comes from the coenzyme FADHOOH is found in the product. (4) Groups Gly132/Ala133/Leu134, Met375/Gln376 and a water fence facilitate the hydroxylation reaction while Leu160/Val161/Ser162 suppresses it. (5) Ser162 suppresses the hydroxylation reaction most, while Leu134 and Gln376 contribute equally in facilitating it.

Acknowledgements

This work was supported by NSFC (National Natural Science Foundation of China, project No. 21177077, 21177076) and Independent Innovation Foundation of Shandong University (IIFSDU, project No. 2012JC030).

Appendix A. Supplementary data

Supplementary data associated with this article can be found, in the online version, at http://dx.doi.org/10.1016/j.jmgm.2013.04.008.

References

[1] R.N. Jones, R.S. Hare, F.J. Sabatelli, In vitro grampositive antimicrobial activity of evernimicin (SCH 27899), a novel oligosaccharide, compared with other antimicrobials: a multicentre international trial, Journal of Antimicrobial Chemotherapy 47 (2001) 15–25.
[2] S. Terakubo, H. Takemura, H. Yamamoto, H. Ikejima, H. Kunishima, K. Kanemitsu, M. Kaku, J. Shimada, Antimicrobial activity of everninomicin against clinical isolates of *Enterococcus* spp., *Staphylococcus* spp., and *Streptococcus* spp. tested by Etest, Journal of Infection and Chemotherapy 7 (2001) 263–266.
[3] R. Jorge, A. Josep, V. Antoni, R. Jordi, New developments in therapeutic agents for Legionnaires' disease, Anti-Infective Agents in Medicinal Chemistry 6 (2007) 228–242.
[4] F.M. Poulet, R. Veneziale, P.M. Vancutsem, P. Losco, K. Treinen, R.E. Morrissey, Ziracin-induced congenital urogenital malformations in female rats, Toxicologic Pathology 33 (2005) 320–328.
[5] S. Nakashio, H. Iwasawa, F.Y. Dun, K. Kanemitsu, J. Shimada, Everninomicin, a new oligosaccharide antibiotic: its antimicrobial activity, post-antibiotic effect and synergistic bactericidal activity, Drugs under Experimental and Clinical Research 21 (1995) 7–16.
[6] A.K. Ganguly, V.M. Girijavallabhan, G.H. Miller, O.Z. Sarre, Chemical modification of everninomicins, Journal of Antibiotics 35 (1982) 561–570.
[7] R. Winkler, C. Hertweck, Biosynthesis of nitro compounds, ChemBioChem 8 (2007) 973–977.
[8] K.S. Ju, R.E. Parales, Nitroaromatic compounds, from synthesis to biodegradation, Microbiology and Molecular Biology Reviews 74 (2010) 250–272.
[9] W.J.H. van Berkel, N.M. Kamerbeek, M.W. Fraaije, Flavoprotein monooxygenases, a diverse class of oxidative biocatalysts, Journal of Biotechnology 124 (2006) 670–689.
[10] V. Joosten, W.J.H. van Berkel, Flavoenzymes, Current Opinion in Chemical Biology 11 (2007) 195–202.
[11] J.L. Vey, A.A. Mestarihi, Y. Hu, M.A. Funk, B.O. Bachmann, T.M. Iverson, Structure and mechanism of ORF36, an amino sugar oxidizing enzyme in everninomicin biosynthesis, Biochemistry 49 (2010) 9306–9317.
[12] H.M. Senn, W. Thiel, QM/MM Methods for biomolecular systems, Angew and Techemie-International Edition 48 (2009) 1198–1229.
[13] L. Ridder, J.N. Harvey, I.M.C.M. Rietjens, J. Vervoort, A.J. Mulholland, Ab Initio QM/MM modeling of the hydroxylation Step in *p*-hydroxybenzoate hydroxylase, Journal of Physical Chemistry B 107 (9) (2003) 2118–2126.
[14] H.M. Senn, S. Thiel, W. Thiel, Enzymatic Hydroxylation in *p*-hydroxybenzoate hydroxylase: a case study for QM/MM molecular dynamics, Journal of Chemical Theory and Computation 1 (2005) 494–505.
[15] R.A. Mata, H.J. Werner, S. Thiel, W. Thiel, Toward accurate barriers for enzymatic reactions: QM/MM case study on *p*-hydroxybenzoate hydroxylase, Journal of Chemical Physics 128 (2008) 025104.
[16] N.A. Bruender, J.B. Thoden, H.M. Holden, X-ray structure of KijD3, a key enzyme involved in the biosynthesis of D-kijanose, Biochemistry 49 (2010) 3517–3524.
[17] K.P. Battaile, T.V. Nguyen, J. Vockley, J.J.P. Kim, Structures of isobutyryl-CoA dehydrogenase and enzyme–product complex, Journal of Biological Chemistry 279 (2004) 16526–16534.
[18] W. Humphrey, A. Dalke, K. Schulten, MD-visual molecular dynamics, Journal of Molecular Graphics 14 (1996) 33–38.
[19] B.R. Brooks, R.E. Bruccoleri, B.D. Olafson, D.J. States, S. Swaminathan, M. Karplus, CHARMM: a program for macromolecular energy, minimization, and dynamics calculations, Journal of Computational Chemistry 4 (1983) 187–217.
[20] B.R. Brooks, C.L. Brooks III, A.D. Mackerell, L. Nilsson, R.J. Petrella, B. Roux, Y. Won, G. Archontis, C. Bartels, S. Boresch, A. Caflisch, L. Caves, Q. Cui, A.R. Dinner, M. Feig, S. Fischer, J. Gao, M. Hodoscek, W. Im, K. Kuczera, T. Lazaridis, J. Ma, V. Ovchinnikov, E. Paci, R.W. Pastor, C.B. Post, J.Z. Pu, M. Schaefer, B. Tidor, R.M. Venable, H.L. Woodcock, X. Wu, W. Yang, D.M. York, M. Karplus, CHARMM: the biomolecular simulation Program, Journal of Computational Chemistry 30 (2009) 1545–1615.
[21] A.D. MacKerell Jr., B. Brooks, C.L. Brooks III, L. Nilsson, B. Roux, Y. Won, M. Karplus, CHARMM: the energy function and its parameterization with an overview of the program, The Encyclopedia of Computational Chemistry 1 (1998) 271–277.
[22] A.D. MacKerell, D. Bashford, M. Bellott, R.L. Dunbrack, J.D. Evanseck, M.J. Field, All-atom empirical potential for molecular modeling and dynamics studies of proteins, Journal of Physical Chemistry B 102 (1998) 3586–3616.
[23] W.L. Jorgensen, J. Chandrasekhar, J.D. Madura, R.W. Impey, M.L. Klein, Comparison of simple potential functions for simulating liquid water, Journal of Chemical Physics 79 (1983) 926–935.
[24] C.L. Brooks, M. Karplus, Deformable stochastic boundaries in molecular dynamics, Journal of Chemical Physics 79 (1983) 6312–6325.
[25] P. Sherwooda, A.H.D. Vriesa, M.F. Guesta, G. Schreckenbacha, C.R.A. Catlowb, S.A. Frenchb, A.A. Sokolb, S.T. Bromleyb, W. Thielc, A.J. Turnerc, S. Billeterc, F. Terstegenc, S. Thielc, J. Kendrickd, S.C. Rogersd, J. Cascie, M. Watsone, F. Kinge, E. Karlsenf, M. Sjovollf, A. Fahmif, A. Schaferg, C. Lennartzg, QUASI: a general-purpose implementation of the QM/MM approach and its application to problems in catalysis, Journal of Molecular Structure-Theochem 632 (2003) 1–28.
[26] R. Ahlrichs, M. Bär, M. Häser, H. Horn, C. Kölmel, Electronic structure calculations on workstation computers: the program system turbomole, Chemical Physics Letters 162 (1989) 165–169.
[27] W. Smith, T.R. Forester, DL_POLY_2.0: a general-purpose parallel molecular dynamics simulation package, Journal of Molecular Graphics & Modelling 14 (1996) 136–141.
[28] A.H. de Vries, P. Sherwood, S.J. Collins, A.M. Rigby, M. Rigutto, G.J. Kramer, Zeolite structure and reactivity by combined quantum-chemical-classical calculations, Journal of Physical Chemistry B 103 (1999) 6133–6141.
[29] D. Bakowies, W.J. Thiel, Hybrid models for combined quantum mechanical and molecular mechanical approaches, Physical Chemistry 100 (1996) 10580–10594.
[30] D. Axel, Becke, A new mixing of Hartree-Fock and local density-functional theories, Journal of Chemical Physics 98 (1993) 1372–1377.
[31] C. Lee, W. Yang, R.G. Parr, Development of the Colle-Salvetti correlation-energy formula into a functional of the electron density, Physical Review B 37 (1988) 785–789.
[32] A.D. MacKerell Jr., D. Bashford, M. Bellott, R.L. Dunbrack Jr., J.D. Evanseck, M.J. Field, S. Fischer, J. Gao, H. Guo, S. Ha, D. Joseph-McCarthy, L. Kuchnir, K. Kuczera, F.T.K. Lau, C. Mattos, S. Michnick, T. Ngo, D.T. Nguyen, B. Prodhom, W.E. Reiher III, B. Roux, M. Schlenkrich, J.C. Smith, R. Stote, J. Straub,

M. Watanabe, J. Wio'rkiewicz-Kuczera, D. Yin, M. Karplus, All-atom empirical potential for molecular modeling and dynamics studies of proteins, Journal of Physical Chemistry B 102 (1998) 3586–3616.
[33] S.R. Billeter, A.J. Turner, W. Thiel, Linear scaling geometry optimization and transition state search in hybrid delocalised internal coordinates, Physical Chemistry Chemical Physics 2 (2000) 2177–2186.
[34] J. Baker, An algorithm for the location of transition states, Journal of Computational Chemistry 7 (1986) 385–395.
[35] D.C. Liu, J. Nocedal, On the limited memory BFGS method for large scale optimization, Journal of Mathematical Programming 45 (1989) 503–528.
[36] I. Polyak, M.T. Reetz, W. Thiel, Quantum mechanical/molecular mechanical study on the mechanism of the enzymatic Baeyer-Villiger reaction, Journal of the American Chemical Society 134 (2012) 2732–2741.
[37] X. Biarnes, A. Ardevol, J. Iglesias-Fernandez, A. Planas, C. Rovira, Catalytic itinerary in 1,3-1,4-β-glucanase unraveled by QM/MM metadynamics. charge is not yet fully developed at the oxocarbenium ion-like transition state, Journal of the American Chemical Society 133 (2011) 20301–20309.
[38] L. Petersen, A. Ardevol, C. Rovira, P.J. Reilly, Mechanism of cellulose hydrolysis by inverting GH8 endoglucanases: a QM/MM metadynamics study, Journal of Physical Chemistry B 113 (2009) 7331–7339.